

# Chapter 1

## Morphological Template Matching in Color Images

Sébastien Lefèvre, Erchan Aptoula, Benjamin Perret, and Jonathan Weber

**Abstract** Template matching is a fundamental problem in image analysis and computer vision. It has been addressed very early by Mathematical Morphology, through the well-known Hit-or-Miss Transform. In this chapter, we review most of the existing works on this morphological template matching operator, from the standard case of binary images to the (not so standard) case of grayscale images and the very recent extensions to color and multivariate data. We also discuss the issues raised by the application of the HMT operator to the context of template matching and provide guidelines to the interested reader. Various use cases in different application domains have been provided to illustrate the potential impact of this operator.

**Key words:** Mathematical morphology, Hit-or-Miss Transform, Template Matching, Color images

---

Sébastien Lefèvre  
Université de Bretagne-Sud, IRISA, e-mail: sebastien.lefeuvre@univ-ubs.fr

Erchan Aptoula  
Okan University, e-mail: erchan.aptoula@okan.edu.tr

Benjamin Perret  
Université Paris-Est, Laboratoire d’Informatique Gaspard-Monge, Equipe A3SI, ESIEE Paris, e-mail: b.perret@esiee.fr

Jonathan Weber  
Université de Lorraine, LORIA-UMR 7503, e-mail: jonathan.weber@univ-lorraine.fr

## 1.1 Introduction

Mathematical Morphology is a very popular toolbox dating back to the 1960s and has achieved great successes. At its early years, mathematical morphology was dedicated to binary images. Binary morphological operators, while still very common in any digital image processing pipeline, are often applied in a second stage (*e.g.*, after a first thresholding step). The extension of mathematical morphology to grayscale images, both from theoretical and practical sides, is now mature after 20 years of developments in the field. It has broadened the possible uses of morphological operators and makes mathematical morphology a first-choice solution for digital image processing [36]. Multivariate images, such as color or multispectral images however constitute a more challenging task. Which is why multivariate mathematical morphology has been addressed only recently, mainly during the last decade. Despite being a recent research field, color morphology has been extensively explored and has led to many advances. As a matter of fact, several review papers or book chapters [2, 4, 5, 1] have already been published on this hot topic.

Our goal here is not to provide *yet another review on color morphology*. We rather focus on a specific problem fairly well addressed by mathematical morphology, namely template matching. Indeed, from the early years of mathematical morphology, this problem has been tackled with a morphological operator called the Hit-or-Miss Transform (HMT). The HMT has been widely used with binary images, relying on a simple pair of patterns to fit the foreground (object) and the background. Its use with grayscale images is more recent [31, 34, 23, 8] and has not yet reached the general image processing community. The various existing approaches for graylevel HMT have been recently reviewed by Murray and Marshall in [22]. The extension of the HMT to color or multispectral images has been achieved only very recently [2, 37, 19, 38] and is still at a preliminary stage of dissemination, while offering a great potential for color image processing. In this chapter, we thus aim to explore in a comprehensive way morphological template matching through the HMT, from the standard binary case to the most recent color extensions.

The organization of the chapter is the following. We first recall the initial definition of the HMT in the binary case (Sec. 1.2), before addressing the case of grayscale images (Sec. 1.3). We then further proceed to color images, and review the different HMT definitions proposed in the literature so far (Sec. 1.4). Each of these parts is provided with the necessary background in order to make the chapter self-contained. In Sec. 1.5, we discuss the implementation issues to be solved when using HMT for practical template matching applications. Such existing applications are then reviewed in Sec. 1.6. Sec. 1.7 concludes this chapter and provides suggestions for future research directions.

## 1.2 Template Matching in Binary Images

In this section, we recall the basics of Mathematical Morphology in the binary case, with adequate definitions and notations. The HMT on binary images will then be presented and discussed, with comprehensive examples.

### 1.2.1 Binary Mathematical Morphology

Let  $E$  be an Euclidean or digital space (*i.e.*  $E = \mathbb{R}^n$  or  $E = \mathbb{Z}^n$  with  $n \in \mathbb{N}^*$ ). Let  $X$  be a subset of  $E$ . Let  $\mathcal{P}(X)$  denote the class of all subsets of  $X$ :  $\mathcal{P}(X) = \{Y \subseteq X\}$ . Let  $X^c$  denote the complement of  $X$ , *i.e.* the set of all points of  $E$  that do not belong to  $X$ :  $X^c = \{y \in E \mid y \notin X\}$ . Let  $\tilde{X}$  denote the reflection of  $X$ , *i.e.* the set  $X$  transformed by a central symmetry:  $\tilde{X} = \{-x \mid x \in X\}$ . Finally, we will denote by  $X_p$  the translate of  $X$  by  $p \in E$  defined by  $X_p = \{x + p \mid x \in X\}$ .

The basic operators of erosion and dilation of  $X$  by the Structuring Element (SE)  $B \in \mathcal{P}(E)$  are written respectively  $\varepsilon_B(X)$  and  $\delta_B(X)$ . They are defined using the Minkowski subtraction ( $\ominus$ ) and addition ( $\oplus$ ):

$$\varepsilon_B(X) = X \ominus B = \bigcap_{b \in B} X_{-b} \quad (1.1)$$

$$\delta_B(X) = X \oplus B = \bigcup_{b \in B} X_b \quad (1.2)$$

### 1.2.2 Binary HMT

Being given a subset  $X$  of  $E$ , the principle of the HMT is to look for all positions  $p$  in  $X$  where a structuring element  $F$  called the *foreground* fits in the shape ( $F_p \subseteq X$ ) while another structuring element  $B$  called the *background* fits in the complement of  $X$  ( $B_p \subseteq X^c$ ). The HMT of  $X$  by the structuring elements  $(F, B)$ , noted  $\text{HMT}_{F,B}(X)$ , can be defined in terms of Minkowski subtraction and addition (structuring erosion and dilation):

$$\begin{aligned} \text{HMT}_{F,B}(X) &= \{p \in X \mid F_p \subseteq X \text{ and } B_p \subseteq X^c\} \\ &= \{p \in X \mid F_p \subseteq X \subseteq B_p^c\} \\ &= (X \ominus F) \cap (X^c \ominus B) \\ &= \varepsilon_F(X) / \delta_{\tilde{B}}(X) \end{aligned} \quad (1.3)$$

A direct consequence of this definition is that if  $F$  and  $B$  have a non-empty intersection, then  $\text{HMT}_{F,B}(X)$  is empty for all  $X$  in  $\mathcal{P}(E)$  (a given pixel cannot simultaneously belongs to the foreground and to the background). One can also note that:

first, the second formulation of Eq.(1.3) is known as the *interval operator* from [15] and second, the complementation does not appear in the last formulation which allows to naturally extend the HMT to gray-level images where complementation is not defined.

Fig. 1.1 illustrates the application of the hit-or-miss transform on a binary image. Our goal here is to detect  $3 \times 3$  squares with possible extensions along edges. It is noteworthy that the two structuring elements do not need to cover the whole neighborhood of a pixel and some pixels, as the middle of the edges of the square, can be excluded from the decision process by neither putting them in  $F$  nor in  $B$ . This is a first attempt to ensure robustness to uncertainty or noise. Some more advanced solutions, not specific to binary images will be reviewed in Sec. 1.5.

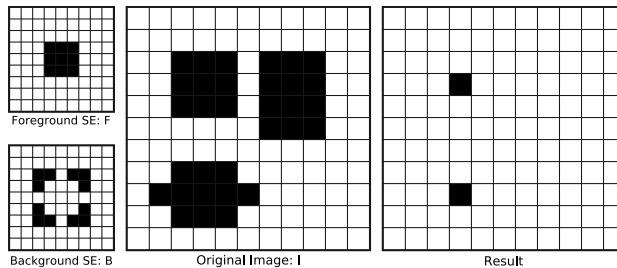


Fig. 1.1: Example of application of binary HMT to detect  $3 \times 3$  squares with possible extensions [27]. The pixels belonging to the images are in black while those belonging to the complement are in white. The top left image represents the foreground SE:  $F$ , origin of the image is at the centre of the square. The bottom left image is the background SE  $B$ , with same origin as  $F$ . The middle image is the original image  $I$ . And the right image is the result of the HMT applied on  $I$  with SEs  $F$  and  $B$ .

### 1.3 Template Matching in Grayscale Images

We recall here basics of Mathematical Morphology in the grayscale case, with adequate definitions and notations. The various definitions of the HMT on grayscale images (*e.g.*, [31, 34, 23, 8]) will then be presented and discussed, with comprehensive examples.

#### 1.3.1 Grayscale Mathematical Morphology

We now consider the case of grayscale images, *i.e.* of mappings from  $E$  to the set of values  $T$  ( $T^E$ ). Moreover, we assume that  $T$  is a complete lattice, *i.e.* a non empty set equipped with a partial ordering  $\leq$ , an infimum  $\wedge$  and a supremum  $\vee$  such that

the infimum and supremum of any non empty subset of  $T$  belongs to  $T$  (for all  $A \subseteq T$ ,  $\bigwedge A \in T$  and  $\bigvee A \in T$ ). The lattice  $T$  is thus bounded by its least element  $\perp = \bigwedge T$  and its greatest element  $\top = \bigvee T$ . For grayscale images we usually take  $T = \overline{\mathbb{R}} = \mathbb{R} \cup \{-\infty, \infty\}$  or  $T = \overline{\mathbb{Z}} = \mathbb{Z} \cup \{-\infty, \infty\}$ . The notion of structuring element naturally extends to the one of structuring function (SF) which is simply an element of  $T^E$ .

The definitions of the binary erosion (Eq. 1.1) and binary dilation (Eq. 1.2) then naturally extend to grayscale images. Let  $F$  in  $T^E$  be a grayscale image and  $V$  in  $T^E$  be a structuring function. The grayscale erosion  $\varepsilon_V(F)$  and dilation  $\delta_V(F)$  of  $F$  by  $V$  are then defined for all  $p \in E$  by:

$$\varepsilon_V(F)(p) = \bigwedge_{x \in \text{supp}(V)} \{F(p+x) - V(x)\} \quad (1.4)$$

$$\delta_V(F)(p) = \bigvee_{x \in \text{supp}(V)} \{F(p-x) + V(x)\} \quad (1.5)$$

where  $\text{supp}(V)$  is the *support* of  $V$ , *i.e.* the set of points of  $E$  where  $V$  is greater than the least element  $\perp$ :  $\text{supp}(V) = \{p \in E \mid V(p) \neq \perp\}$ . These formulas can lead to disinclination like  $+\infty$  plus  $-\infty$ . To keep consistency  $+\infty$  plus  $-\infty$  must be valued as  $-\infty$  in Eq. 1.5 and as  $+\infty$  in Eq. 1.4.

### 1.3.2 Grayscale HMT

The binary HMT was first extended to grayscale images by Ronse [31] and then many other definitions followed: by Shaefer [32], Khosravi [18], Raducanu [29], Soille [36], Barat [7], Perret [27]. A recent survey on grayscale HMT is given in [22]. These various definitions have been recently unified into a common theoretical framework for graylevel *interval operators* [23]. In the binary case, the interval operator (second line of Eq.1.3) looks for each translation  $p \in E$  if the image fits between the background SE translated at  $p$  and the complement of the background SE also translated at  $p$ . In the grayscale case, the sought template is translated not only horizontally (by a point  $p \in E$ ), but vertically as well (by a finite graylevel  $t \in T$ ) in an attempt to detect the positions where it fits (Fig. 1.2). Specifically, we will note  $V_{(p,t)}$  the translation of  $V \in T^E$  by a couple  $(p,t) \in E \times T$ : for all  $x \in E$ ,  $V_{(p,t)}(x) = V(x-p) + t$ .

According to the unified theory for grayscale HMT [23], a grayscale HMT is decomposed into two stages:

- the *fitting*, where the locations fitting the given structuring functions, describing the sought template, are computed,
- and *valuation*, where the resulting image containing the previously detected locations is constructed.

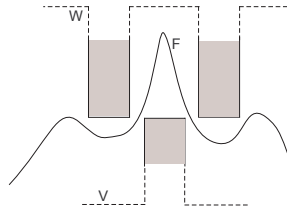


Fig. 1.2: The integral interval operator, Eq. (1.13) [6].

Let us observe that in the binary case, the fitted pixels are the ones retained by the HMT, and their valuation is simply equal to 1 (or foreground).

### 1.3.2.1 Fitting

We first describe the different fittings. Let  $F \in T^E$  be a grayscale image and  $V, W \in T^E$  be a couple of structuring functions describing the sought template such that  $V \leq W$ . Formally a fitting is a mapping from  $T^E$  into  $\mathcal{P}(E \times T')$  where  $T'$  can be a subset of  $T$  or any set of values. A first fitting involved in Ronse's HMT is given by:

$$H_{V,W}(F) = \{(p,t) \in E \times T \mid V_{(p,t)} \leq F \leq W_{(p,t)}\} \quad (1.6)$$

$$= \{(p,t) \in E \times T \mid \varepsilon_V(F)(p) \leq t \leq \delta_{W^*}(F)(p)\} \quad (1.7)$$

where  $W^* : x \rightarrow -W(-x)$ , is the *dual* of  $W$ .  $H_{V,W}(F)$  is thus the set of all translations where the image lies between both structuring functions (Fig. 1.3). A second fitting,

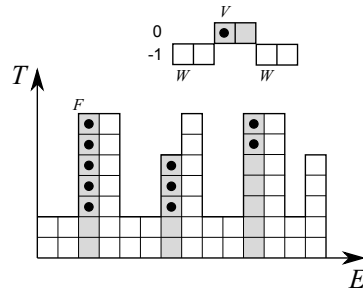


Fig. 1.3: Illustration of  $H_{V,W}$  (Eq. (1.6)). We consider a function  $F$  from  $E = \mathbb{Z}$  into  $T = \overline{\mathbb{Z}}$  and the two structuring functions  $V$  and  $W$  (the origin is on the left pixel of  $V$ ). The result of  $H_{V,W}(F)$  is the set of points of  $E \times T$  marked by a black circle inside  $F$ . We also give the result of the application of the supremal valuation (Eq. (1.12)) of  $H_{V,W}(F)$  in gray, i.e. the result of  $RHMT_{V,W}(F)$  (Eq. (1.14)).

involved in Soille's and Barat's HMT is:

$$K_{V,W}(F) = \{(p,t) \in E \times T \mid V_{(p,t)} \leq F \ll W_{(p,t)}\} \quad (1.8)$$

$$= \{(p,t) \in E \times T \mid \varepsilon_V(F)(p) \leq t < \delta_{W^*}(F)(p)\} \quad (1.9)$$

where  $F \ll W$  means that there is some  $h > 0$  such that for every  $p \in E$  we have  $F(p) \leq W(p) - h$ .  $K_{V,W}(F)$  is thus the set of all translations where the image lies between both structuring functions and does not touch  $W$  (Fig. 1.4).

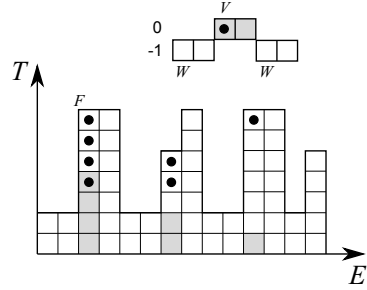


Fig. 1.4: Illustration of  $K_{V,W}$  (Eq. (1.8)). We consider a function  $F$  from  $E = \mathbb{Z}$  into  $T = \overline{\mathbb{Z}}$  and the two structuring functions  $V$  and  $W$  (the origin is on the left pixel of  $V$ ). The result of  $K_{V,W}(F)$  is the set of points of  $E \times T$  marked by a black circle inside  $F$ . We also give the result of the application of the integral valuation (Eq. (1.13)) of  $K_{V,W}(F)$  in gray, i.e. the result of  $SHMT_{V,W}(F)$  (Eq. (1.15)).

Finally, a third fitting involved in Perret's HMT is given by:

$$P_{V,W}(F) = \left\{ p, \frac{|\{q \in S \mid V(q) + t \leq F(p+q) \leq W(q) + t\}|}{|S|} \in E \times [0, 1] \mid t \in T \right\} \quad (1.10)$$

where  $S = \{x \in E \mid V(x) \neq \perp \text{ or } W(x) \neq \top\}$  and  $|X|$  is the cardinal of the set  $X$ . Hence,  $P_{V,W}(F)$  does not look for locations where both structuring functions completely fit the image. Instead, it measures at each location how well both structuring functions fit the image by counting, among the points of the image that lies in the support of one of the SF, the ratio of points that fits between both SF (Fig. 1.5).

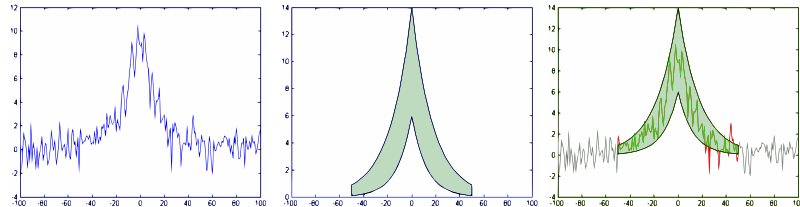


Fig. 1.5: Example of application of the  $P_{V,W}(F)$  (Eq. 1.10) to detect an exponential profile with Gaussian noise [27]. The first image represents a 1D noisy signal. The second image represents the uncertainty area defined by the 2 SFs  $V$  (lower function) and  $W$  (upper function). The third image shows how well the pattern can fit the signal.

### 1.3.2.2 Valuation

Likewise, there are several types of valuations. Formally, a valuation  $\eta$  is a mapping that associates a (grayscale) image ( $T^E$ ) to any result of a fitting ( $\mathcal{P}(E \times T')$ ). Let  $Y \in \mathcal{P}(E \times T')$ , the simplest valuations  $\eta^B(Y)$ , the *binary* valuation, consists in taking the set of points  $p \in E$  for which there is at least one  $t \in T$  such that  $(p, t)$  belongs to  $Y$ .

$$\eta^B(Y)(p) = \begin{cases} 1 & \text{if } \exists t \in T', (p, t) \in Y \\ 0 & \text{otherwise} \end{cases}. \quad (1.11)$$

Another valuation is the *supremal* valuation  $\eta^S(Y)$ , which for every point  $p \in E$  of fit couples  $\{(p, t)\} \subseteq Y$ , takes the supremum of  $t$  (Fig. 1.3):

$$\eta^S(Y)(p) = \sup \{t \mid (p, t) \in Y\} \quad (1.12)$$

Finally there is the *integral* valuation  $\eta^I(Y)$  which instead for every point  $p$  of fit couples  $\{(p, t)\} \subseteq Y$ , uses the length of the interval of  $t$  for which the couples  $(p, t)$  fit (Fig. 1.4).

$$\eta^I(Y)(p) = \text{mes} \{t \mid (p, t) \in Y\} \quad (1.13)$$

where  $\text{mes}$  is an appropriate measure of intervals in  $T'$  (simply the Lebesgue measure if  $T'$  is an interval of  $\mathbb{R}$  or  $\mathbb{Z}$ ).

### 1.3.3 HMT Definitions

The different combination of fittings and valuations allows to recover the different definitions of HMT. Let  $F, V, W \in T^E$  with  $V \leq W$  and  $p \in E$ , among others, we mention:

$$\begin{aligned} (\text{Ronse}) \text{RHMT}_{V,W}(F)(p) &= \eta^S(H_{V,W}(F))(p) \\ &= \begin{cases} \varepsilon_V(F)(p) & \text{if } \varepsilon_V(F)(p) \geq \delta_{W^*}(F)(p), \\ \perp & \text{otherwise} \end{cases} \end{aligned} \quad (1.14)$$

$$\begin{aligned} (\text{Soille}) \text{SHMT}_{V,W}(F)(p) &= \eta^I(K_{V,W}(F))(p) \\ &= \max \{\varepsilon_V(F)(p) - \delta_{W^*}(F)(p), 0\} \end{aligned} \quad (1.15)$$

$$\begin{aligned} (\text{Perret}) \text{PHMT}_{V,W}(F)(p) &= \eta^S(P_{V,W}(F))(p) \\ &= \max_{t \in T} \frac{|\{q \in S \mid V(q) + t \leq F(p+q) \leq W(q) + t\}|}{|S|} \end{aligned} \quad (1.16)$$

Ronse's and Soille's HMT are illustrated in Fig. 1.3 and 1.4 and further compared in Fig. 1.6 while an application of Perret's HMT is given in section 1.6.1.

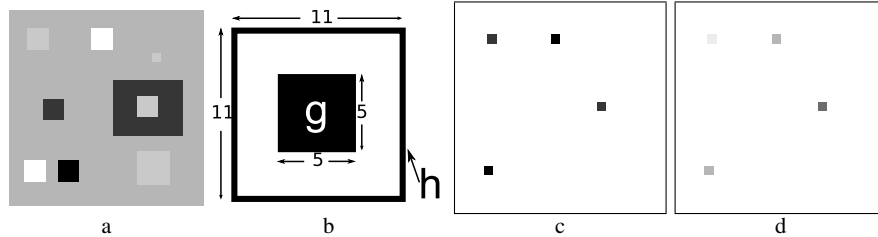


Fig. 1.6: Grayscale HMT : a) original image ( $64 \times 64$  pixels); b) couple of structuring functions used within the HMT; c) result with Ronse's, d) and Soille's definition (results are displayed in inverse gray levels and for the sake of clarity,  $\perp$  value was replaced with 0) [38].

## 1.4 Template Matching in Color and Multivariate Images

The extension of the HMT to color and more generally to multivariate images such as multi- and hyper-spectral data, can amplify the application potential of the operator at a significant level. Of particular importance in this context are applications regarding color object detection from color data, target detection from remote sensing data, as well as the detection of challenging celestial objects from astronomical imaging sources.

However, given the multitude of existing approaches for the definition of the grayscale HMT, it is no surprise that the situation is no less clearer with multivariate images. In fact, conversely to grayscale morphological image processing, there is not even a generally accepted color mathematical morphology framework, let alone a standardized multivariate HMT. Nevertheless, the increasingly widespread availability of multivariate images, especially in the context of remote sensing, as well as recent advances in color morphology, have provided the missing impetus that has led to the intensification of the research work on extending the HMT to color, multi- and hyper-spectral data.

We will start this section by first recalling the basic theoretical implications of using multivariate images to the mathematical morphology theory, and elaborate on the difficulties of its extension to this type of images. Then, we will present the different methods that have been developed especially in the past few years for applying the HMT to multivariate images.

### 1.4.1 Multivariate Mathematical Morphology

According to the lattice based approach to mathematical morphology [30], digital images are represented as mappings  $F : E \rightarrow T$  between the discrete coordinate grid  $E$  and the set of pixel values  $T$ , with  $T$  being a complete lattice. More precisely, imposing a complete lattice structure on an arbitrary set of pixel values  $T$  is possible,

if  $T$  is equipped with at least a partial ordering relation which enables the computation of the infimum and supremum of any non-empty subset of  $T$ . Consequently, the morphological operators can be in fact applied to any type of image data, as long as the set of pixel values  $T$  possesses a complete lattice structure. For a detailed account of multivariate morphology the reader is referred to Refs. [14, 33].

For instance, in the case of continuous multidimensional grayscale images where  $F : \mathbb{R}^d \rightarrow \mathbb{R}$ , it suffices to employ the usual comparison operator  $\leq$ , in order to induce a complete lattice structure on  $\mathbb{R}$ . Likewise, the inclusion operator  $\subseteq$  can be used with binary images  $F : \mathbb{R}^d \rightarrow \{0, 1\}$ . However, if we now consider multivariate images  $F : \mathbb{R}^d \rightarrow \mathbb{R}^n$ ,  $n > 1$ , where  $n = 3$  for the specific case of color images, it becomes problematic to find an ordering relation for the vectors of  $\mathbb{R}^n$ , due to the fact that there is no universal method for ordering multivariate data. As a result, in the last 15 years several ordering approaches have been explored with the end of extending mathematical morphology to multivariate images, for a detailed survey of which the reader is referred to Ref. [2].

We briefly recall the main properties of an ordering, *i.e.* a binary relation  $\leq$  on a set  $\mathcal{T}$  being reflexive ( $\forall x \in \mathcal{T}, x \leq x$ ), anti-symmetric ( $\forall x, y \in \mathcal{T}, x \leq y$  and  $y \leq x \Rightarrow x = y$ ), and transitive ( $\forall x, y, w \in \mathcal{T}, x \leq y$  and  $y \leq w \Rightarrow x \leq w$ ). An ordering is total if the totality statement ( $\forall x, y \in \mathcal{T}, x \leq y$  or  $y \leq x$ ) holds, partial otherwise. It is a pre-ordering if the anti-symmetry statement does not hold.

Hence, the HMT being a morphological tool, its extension to multivariate images also requires the implication of a vector ordering. We will now proceed to examine various solutions developed for applying the HMT to color or to multivariate data in general.

### 1.4.2 HMT Based on a Vectorial Ordering

Aptoula et al. [6] provide the first study on the theoretical requirements of a vectorial HMT (VHMT). In detail, the initial step for extending the HMT to multivariate data, consists in defining the erosion and dilation operators for multivariate images in combination with multivariate structuring functions (SF). More precisely, these operators are based on horizontal translations (by a point  $p \in E$ ) as well as on vertical ones (by a finite pixel value  $\mathbf{t} \in T$ ) as in the grayscale case, the difference is however that pixel values are now multi-dimensional; in particular, given a multivariate image  $\mathbf{F} : E \rightarrow T$ :

$$\forall (p, \mathbf{t}) \in E \times T, \quad \mathbf{F}_{(p, \mathbf{t})}(x) = \mathbf{F}(p - x) + \mathbf{t} \quad (1.17)$$

Furthermore, according to the fundamental Refs. [16, 17] of Heijmans and Ronse, translations need to be complete lattice automorphisms (*i.e.* bijections  $T \rightarrow T$  that preserve order, and whose inverse also preserve order). Consequently, the vector ordering ( $\leq_v$ ) from which the complete lattice is derived, must be translation invariant. In other words:

$$\forall \mathbf{w}, \mathbf{w}', \mathbf{t} \in T, \quad \mathbf{w} \leq_v \mathbf{w}' \Leftrightarrow \mathbf{w} + \mathbf{t} \leq_v \mathbf{w}' + \mathbf{t} \quad (1.18)$$

Thus one can give the definition of the erosion and dilation respectively of a multivariate image  $\mathbf{F}$  by a multivariate SF  $\mathbf{B}$ :

$$\varepsilon_{\mathbf{B}}(\mathbf{F})(p) = \inf_{x \in \text{supp}(\mathbf{B})} \{\mathbf{F}(p+x) - \mathbf{B}(x)\} \quad (1.19)$$

$$\delta_{\mathbf{B}}(\mathbf{F})(p) = \sup_{x \in \text{supp}(\mathbf{B})} \{\mathbf{F}(p-x) + \mathbf{B}(x)\} \quad (1.20)$$

where  $\text{supp}(\mathbf{B}) = \{p \in E \mid \mathbf{B}(p) > \perp\}$ , while  $\inf_v$  and  $\sup_v$  denote respectively the infimum and supremum based on the vector ordering ( $\leq_v$ ) under consideration. Hence, these formulations form an adjunction as demanded by Refs. [16, 17] and besides, with a flat SE (*i.e.*  $\forall x, \mathbf{B}(x) = \mathbf{0}$ ) they are reduced to the flat multivariate erosion and dilation formulations. Furthermore, thanks to Eq. (1.18), both fitting equivalences between Eqs. (1.6) and (1.7) as well as between Eqs. (1.8) and (1.9) become directly extendable to this case by replacing the grayscale operators with their multivariate counterparts. As to valuation, the same options as before are available, however the supremum is of course now computed among vectors through the vector ordering in use. In the case of integral valuation, a vector distance now can be used in order to measure the distance among the vectors that have fit. Consequently one can express the multivariate versions of the integral and supremal interval operators respectively as follows:

$$\eta_{[\mathbf{V}, \mathbf{W}]}^I(\mathbf{F})(p) = \begin{cases} \|\varepsilon_{\mathbf{V}}(\mathbf{F})(p) - \delta_{\mathbf{W}^*}(\mathbf{F})(p)\| & \text{if } \varepsilon_{\mathbf{V}}(\mathbf{F})(p) >_v \delta_{\mathbf{W}^*}(\mathbf{F})(p) \\ 0 & \text{otherwise.} \end{cases} \quad (1.21)$$

$$\eta_{[\mathbf{V}, \mathbf{W}]}^S(\mathbf{F})(p) = \begin{cases} \varepsilon_{\mathbf{V}}(\mathbf{F})(p) & \text{if } \varepsilon_{\mathbf{V}}(\mathbf{F})(p) \geq_v \delta_{\mathbf{W}^*}(\mathbf{F})(p) \\ \perp & \text{otherwise.} \end{cases} \quad (1.22)$$

where  $\mathbf{V} \leq_v \mathbf{W}$ . As far as  $\eta^I$  is concerned, it provides a non-zero output at positions where  $\mathbf{V} \leq_v \mathbf{F} \ll_v \mathbf{W}$  according to the ordering in use. It should also be noted that the grayscale valuation choice by means of the Euclidean norm ( $\|\cdot\|$ ) is arbitrary, and a multi-dimensional valuation is of course possible. As to  $\eta^S$ , it produces a non-zero output at positions where  $\mathbf{V} \leq_v \mathbf{F} \leq_v \mathbf{W}$ .

Therefore, the only obstacle preventing the definition of a VHMT is a translation preserving vector ordering. This useful property, among others, is provided by the standard *lexicographical ordering* which is frequently employed in the context of multivariate morphology [3]:

$$\forall \mathbf{v}, \mathbf{v}' \in \mathbb{R}^n, \quad \mathbf{v} <_L \mathbf{v}' \Leftrightarrow \exists i \in \{1, \dots, n\}, \quad (\forall j < i, v_j = v'_j) \wedge (v_i < v'_i) \quad (1.23)$$

while for instance its recent variation  $\alpha$ -modulus lexicographical [1], does not provide it. Moreover, the chosen ordering directly affects the behavior of VHMT. For instance, in the case of lexicographical ordering, which is known for its tendency of prioritising the first vector component [3], this property can be observed in the detection process of VHMT. In particular, during the fitting stage where the erosion

and dilation outputs are computed, since it is the first vector component that decides the outcome of the majority of lexicographical comparisons, fitting the first channel of the vectorial structuring function becomes more important with respect to the rest. This example is illustrated in Fig. 1.7, where although only  $V_1 \leq F_1$ , according to the lexicographical ordering,  $\mathbf{V} <_L \mathbf{F}$ . This property for example would allow for a prioritised detection, where a color template is searched with more emphasis on its brightness than its saturation. A more practical example of VHMT is given

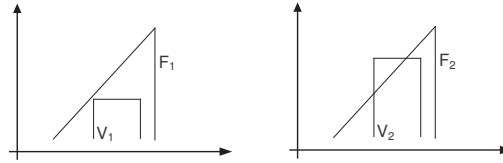


Fig. 1.7: A two-channel image  $\mathbf{F} = (F_1, F_2)$  and a vectorial structuring function  $\mathbf{V} = (V_1, V_2)$  [6].

in Fig. 1.8, where the yellow sign of the middle is sought using a lexicographical (pre-)ordering in the LSH color space where saturation (S) is compared after luminance (L) and hue does not participate in comparisons due to its periodicity. More precisely, the SF positioned under the object ( $\mathbf{V}$ ) is formed by decreasing the pixel values of the template by a fixed amount (e.g., 3, if pixel values are in  $[0, 255]$ ), whereas the background SF ( $\mathbf{W}$ ) is formed by increasing it. Hence, the operator looks for all objects that fit between the upper and lower SF based on the lexicographical principle. In this particular case, as the hue is not taken into account, it detects the left sign despite its different hue value, while it misses the right sign, even though its only difference from the template are a few white points; a result that asserts the sensitivity of the operator. Robustness to noise will be specifically addressed in Sec. 1.5.

### 1.4.3 HMT Based on Multiple Structuring Elements

In multivariate images, template matching can benefit from user knowledge both on spatial and spectral point of views. The main difficulty faced by template matching operators (such as the morphological hit-or-miss transform) is how to combine these two kinds of information. While the spatial information such as the shape and the size of the sought object can be easily provided by a user, its combination with spectral information is not trivial. Moreover, when dealing with complex patterns, defining a single pair of structuring elements or even functions may be very challenging for the user.

Thus Weber and Lefèvre [38] propose another strategy to design the structuring elements. When seeking for a predefined complex template, the user is then

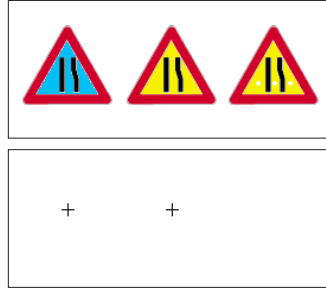


Fig. 1.8: In the first row are three images, of which the middle is the sought pattern. The second row shows the locations where it was detected by Eq. (1.21) based on a lexicographical ordering of luminance and saturation [6].

assumed to be able to describe this template by a set of elementary units. Each of these units describes a particular feature of the template, combining some spatial and spectral information. More precisely, it consists of an expected spectral response in some spatial area. To represent such a knowledge, each particular feature is defined by an extended structuring element combining spatial properties (shape and size of the area where spectral knowledge is available) provided by the structuring element similarly to existing HMT definitions, and spectral information consisting of an expected intensity or value in a given spectral band. Thus it can be either lower or higher bounded by a predefined threshold (*i.e.* definition as a background or foreground template), resulting in three spectral properties for each structuring element: the spectral band it is related to, the kind of threshold used (either low or high threshold) and the threshold value.

Contrary to the standard definition of the HMT, a set of extended structuring elements (not necessarily only two) to be involved in the matching process is considered in this approach. While this method deals with spatial information similarly to previous approaches, a particular attention is given to the spectral information. Indeed, contrary to the previous vectorial definition, each extended structuring element used here is dedicated to a single spectral band. By this way, the user can more easily design the set of structuring elements based on prior knowledge on the sought template. The use of low and high thresholds helps to ensure the robustness of the template matching process, and provides a more practical and realistic way to formulate prior spectral knowledge (compared to previous definitions which are rather contrast-based operators) and may be seen somehow as a generalization of the initial HMT.

For a given extended structuring element  $k$  from the set  $K$ , the spatial pattern (combining shape and size information) is written  $F_k$ , the spectral band  $b_k$ , the threshold or bound  $t_k$  and the related operator (which can be either dilation  $\delta$  or erosion  $\varepsilon$ , corresponding respectively to a high or low threshold, or in other words to foreground or background SE)  $\phi_k$ . The spatial pattern is not expected to be constant

over the different image bands. Of course several extended structuring elements may consider the same spectral band, under the assumption that they are consistent together. Conversely, some image band might be of no interest for a given template matching task and thus not be related to any SE. The fitting step consists of checking, for each analyzed pixel, if its neighbourhood matches the set of extended structuring elements. A pixel will be matched if and only if its neighbourhood fits all the structuring elements, *i.e.* the following condition holds:

$$\text{KHMT}_K(\mathbf{w})(\mathbf{p}) \text{ fits iff } \forall k \in K, \quad \begin{cases} \varepsilon_{F_k}(w_{b_k})(\mathbf{p}) \geq t_k, & \text{if } \phi_k = \varepsilon \\ \delta_{F_k}(w_{b_k})(\mathbf{p}) < t_k, & \text{otherwise} \end{cases} \quad (1.24)$$

Other fusion options are available to merge the individual fitting results, but the conjunction is of course to be preferred since it ensures that the proposed operator possesses a consistent behavior with common morphological transforms. Similarly to existing definitions, the fitting is followed by a valuation step which aims at giving a resulting value to all matched pixels (the unmatched pixels are set to  $\perp$ ). But contrary to previous works assuming a single pair of foreground/background (or erosion/dilation) structuring elements, here a whole set of extended structuring elements with various properties (shape and size but also spectral band and threshold value, as well as the threshold or operator type) has to be considered. In order to measure how well a pixel (and its neighbourhood) fits a complete set of extended structuring elements, the proposed solution is to first perform a valuation for each individual structuring element. The quality of each individual fitting procedure is then measured by relying on the erosion or dilation result and the considered threshold, instead of both erosion and dilation as in existing HMT definitions. Thus the difference between the morphologically processed pixel and the threshold is computed:

$$\text{KHMT}_k(\mathbf{w})(\mathbf{p}) = \begin{cases} \varepsilon_{F_k}(w_{b_k})(\mathbf{p}) - t_k, & \text{if } \phi_k = \varepsilon \\ t_k - \delta_{F_k}(w_{b_k})(\mathbf{p}), & \text{otherwise} \end{cases} \quad (1.25)$$

which ensures a strictly positive result for each fitted pixel. However, no assumption can be made that in practice multivariate images will always contain comparable spectral bands. In other words, the different spectral components of a multivariate image may not share the same value ranges. Thus, a normalization step is further introduced, resulting in a new definition for the individual valuation steps:

$$\begin{aligned} \text{KHMT}_k(\mathbf{w})(\mathbf{p}) &= \begin{cases} (\varepsilon_{F_k}(w_{b_k})(\mathbf{p}) - t_k) / (w_{b_k}^+ - t_k), & \text{if } \phi_k = \varepsilon \\ (t_k - \delta_{F_k}(w_{b_k})(\mathbf{p})) / (t_k - w_{b_k}^-), & \text{otherwise} \end{cases} \\ &= \begin{cases} (\varepsilon_{F_k}(w_{b_k})(\mathbf{p}) - t_k) / (w_{b_k}^+ - t_k), & \text{if } \phi_k = \varepsilon \\ (\delta_{F_k}(w_{b_k})(\mathbf{p}) - t_k) / (w_{b_k}^- - t_k), & \text{otherwise} \end{cases} \end{aligned} \quad (1.26)$$

where  $[w_i^-, w_i^+]$  is the predefined value range of the spectral band  $w_i$  (and of course the assumptions  $t_k \neq w_{b_k}^-$  and  $t_k \neq w_{b_k}^+$ ). The normalization is achieved by  $(w_{b_k}^+ - t_k)$  or  $(w_{b_k}^- - t_k)$  in order to obtain a valuation in  $[0, 1]$ . Once the individual valuations have been computed, it is then necessary to assign a unique value to each matched pixel. In addition, there is no unique valuation scheme for this multivariate HMT. Indeed, one can even keep the set of individual valuations as the final result if interested in the quality of the fit for each individual pattern. But usually, a single scalar value is “expected” and it is here built with a fusion rule. To ensure coherence with the previous fitting step (where a conjunction rule has been used to merge individual fitting results), the method relies on a T-norm, *e.g.*, either the product or the minimum, leading respectively to the following definitions:

$$\text{KHMT}_K^{\text{prod}}(\mathbf{w})(\mathbf{p}) = \begin{cases} \prod_{k \in K} (\text{KHMT}_k(\mathbf{w})(\mathbf{p})) & \text{if } \forall k \in K, \text{KHMT}_k(\mathbf{w})(\mathbf{p}) > 0 \\ 0 & \text{otherwise} \end{cases}$$

$$= \prod_{k \in K} \left( \max(\text{KHMT}_k(\mathbf{w})(\mathbf{p}), 0) \right) \quad (1.27)$$

$$\text{KHMT}_K^{\text{min}}(\mathbf{w})(\mathbf{p}) = \begin{cases} \min_{k \in K} (\text{KHMT}_k(\mathbf{w})(\mathbf{p})) & \text{if } \forall k \in K, \text{KHMT}_k(\mathbf{w})(\mathbf{p}) > 0 \\ 0 & \text{otherwise} \end{cases}$$

$$= \min_{k \in K} \left( \max(\text{KHMT}_k(\mathbf{w})(\mathbf{p}), 0) \right) \quad (1.28)$$

Fig. 1.9 illustrates the relevance of this approach in the context of an RGB image containing objects of various shapes (crosses, rectangles, circles and squares) and different colors. The sought template is a cross with a color close to the background color, leading here to three structuring elements (related to the three color bands) to be used by the HMT. For the sake of comparison, the result with the vectorial HMT (based on a lexicographical ordering) is also given.

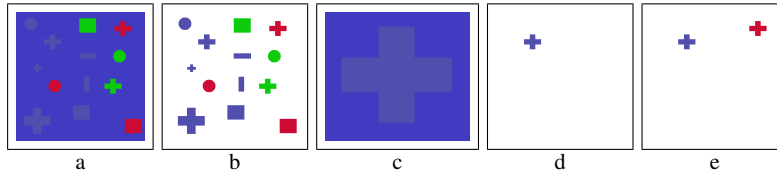


Fig. 1.9: a) Original image; b) Image without background; c) Template to detect (magnified); d) KHMT after reconstruction; e) VHMT with lexicographical ordering after reconstruction [38]

#### 1.4.4 HMT Based on Supervised Ordering

Velasco and Angulo [37] have developed an alternative approach for applying the HMT on multivariate images, using a supervised ordering which is not a total ordering (contrary to lexicographical ordering discussed previously).

As far as the lack of ordering from color vectors is concerned, they rely on the principle of reduced orderings. According to this technique, given a non-empty set  $R$  which lacks a complete lattice structure, one can impose a such structure by means of a mapping  $h : R \rightarrow T$  where  $T$  is complete lattice, which leads to an *h-ordering*  $\leq_h$  [14]:

$$\forall r, r' \in R, \quad r \leq_h r' \Leftrightarrow h(r) \leq h(r') \quad (1.29)$$

An *h-supervised ordering* on the other hand is based on subsets  $B, F \subset R$ , such that  $B \cap F = \emptyset$  and is defined as an h-ordering that satisfies  $h(b) = \perp$  if  $b \in B$  and  $h(f) = \top$  if  $f \in F$ ; where  $\perp$  and  $\top$  represent respectively the minimum and maximum of  $T$ . In which case the resulting h-supervised ordering is denoted by  $h_{\{B,F\}}$ . Given the lack of extremal coordinates within the vector space containing the color vectors, such as black and white with grayscale values, the use of arbitrarily selected  $B$  and  $F$  sets enables the construction of an ordering based on custom extremal coordinates. Ref. [37] relies on Support Vector Machines in this regard, in order to construct a hyperplane separating the vectors that emanate from  $B$  and  $F$ . Thus the vectors are ordered w.r.t. their distance to the maximum margin hyperplane.

Consequently, they redefine the binary HMT using their h-supervised ordering, with  $\{1 = \top, 0 = \perp\}$  and the image complement obtained by exchanging the subsets  $B$  and  $F$ :

$$HMT(I; \{B, F\}, S_1, S_2) = \{x \in E \mid \forall i, \varepsilon_{h_i; S_i}(I(x)) = \top_i\} \quad (1.30)$$

where

$$h_i = \begin{cases} h_{\{B,F\}} & | h(b) = \perp, h(f) = \top \quad \text{if } i = 1; \\ h_{\{F,B\}} & | h(f) = \perp, h(b) = \top \quad \text{if } i = 2; \end{cases} \quad (1.31)$$

and  $\varepsilon_{h_i; S_i}$  denotes the erosion operator with SE  $S_i$  and based on the h-supervised ordering  $h_i$ .

At which stage they extend the binary HMT of Eq.(1.30) to the multivariate case, by associating each vector value set within the sought template SE with a particular  $B_i \subset \mathbb{R}^n$  and using sets of  $\{B_i, S_i\}_{i=1, \dots, k}$  couples such that  $\forall i \neq j, S_i \in E, S_i \cap S_j = \emptyset$ :

$$HMT(I; \{B_i, S_i\}) = \{x \in E \mid \forall i, \varepsilon_{\{B_i, B_{-i}\}; S_i}(I(x)) = \top_i\} \quad (1.32)$$

where  $B_{-i} = \bigcup_{j \neq i} B_j$ ,  $\{S_i\}_{i=1, \dots, k}$  is the family of structuring elements and  $\{B_i\}_{i=1, \dots, k}$  is the family of vectorial pixel values associated with  $\{S_i\}_{i=1, \dots, k}$ .

Finally, in order to achieve robustness against noise the authors have also implemented a more practical version of Eq. (1.32) by using a threshold  $\varepsilon$  controlling the “level” of detection:

$$HMT_\varepsilon(I; \{B_i, S_i\}) = \{x \in E \mid \forall i, dist(\varepsilon_{\{B_i, B_{-i}\}; S_i}(I(x)), \top_i) \leq \varepsilon\} \quad (1.33)$$

with  $dist$  being an arbitrary metric.

#### 1.4.5 HMT Based on Perceptual Color Distance

A further approach focusing on color template matching by means of morphological methods has been recently introduced by Ledoux et al. [19]. The authors base their work on the gray HMT formulation of Barat et al. [7] and propose an extension designed specifically for color images.

In particular, in order to overcome the lack of ordering among color vectors, they propose to use two arbitrary reference color coordinates A and B within the CIELAB color space. In which case given a finite set of color vectors, they suggest computing their maximum as the closest color vector to reference A and the minimum as the closest to reference B. And as far as the metric in place is concerned, they employ the perceptual distance of CIELAB. Consequently, they implement erosion and dilation based on the aforementioned extrema. Thus they employ two distinct pre-orderings; since two unequal color vectors may very well possess the same distance to a reference color, they can both end up being considered equivalent; meaning that distance based ordering approaches of this type lack anti-symmetry.

This theoretical inconvenience however has not hindered the authors from using their color dilation and erosion formulations with template matching purposes. Specifically, they have introduced the *CMOMP* (Color Multiple Object Matching using Probing) [19] tool, which given two structuring functions  $g'$  and  $g''$  representing the lower and higher bounds of the sought template respectively, they associate each pixel  $x$  of the input image  $f$  with the perceptual distance ( $\Delta E$ ) computed at CIELAB between the dilation and erosion outputs at the same coordinate.

$$CMOMP_{g',g''}(f)(x) = \Delta E(\delta_{g''}(f), \varepsilon_{g'}(f)) \quad (1.34)$$

All in all, the CMOMP adopts a similar approach to that in Ref. [37] by employing user specified extremal coordinates for the multi-dimensional color space, with the additional advantage of perceptual color different computation.

In conclusion, although all four color/multivariate HMT approaches presented in this section possess a variety of properties, none of them stands out as the “ultimate” solution to the problem of morphological color template matching; since such an approach would have to be both effective, robust against noise, computation-wise efficient, easy to use/customize and of course possess as many forms of invariance (w.r.t. rotation, scale, illumination, etc.) as possible. All the same, all of the presented approaches have appeared in the past few years, a fact highlighting both the attention that this topic enjoys at the moment as well as asserting future developments. And now, let us focus on the implementation issues related to the HMT.

## 1.5 Implementation of Template Matching Solutions Based on HMT

In the previous sections, we have given a theoretical presentation of the HMT, for binary, grayscale, and color or multivariate images. In order for these definitions to be of practical interest in template matching, several implementation issues have to be considered. We review here the main problems faced by the HMT when applied to template matching. Equipped with the solutions reviewed in this section, the HMT is then able to deal with real template matching use cases, which will be presented next.

### 1.5.1 Robustness to Image Transforms

When a template matching operator is applied in a real context, it is far from an artificial situation and easy to solve problem such as those given in the figures of previous sections. Indeed, it has often to face a great variation both of the template to be matched and its environment. These variations mainly occur due to global, or worse local, image transforms.

Greyscale or spectral image transforms lead to (linear or not) modifications of the template / image pixel values. Most of the HMT definitions reviewed so far are contrast-based operators, *i.e.* they are robust to a global change in pixel values. For methods which are not (*e.g.*, [38]), it is possible to normalize the input image in order to avoid brightness changes. Similarly, in case of varying image contrast, usual techniques in image processing such as histogram equalization or specification become necessary. Since these image dynamics may have different properties over an image (*i.e.* have an effect different in some parts of the image w.r.t. the others), spatially-variant morphological operators are certainly worth being exploited in this context.

Spatial image transforms are various. We distinguish here between translation and scale/orientation. Translation is inherently addressed by Mathematical Morphology which provides translation invariant operators, and thus does not need further discussion. Of course this assumes that the HMT is applied on every single pixel of the image.

The easiest solution to ensure orientation or scale robustness is to apply the template in various configurations corresponding to the possible orientations and scales. This means applying the HMT with a complete set of SE in various orientations and sizes related to the considered configurations. The fitting and valuation steps may be defined as follows: a pixel is fit as soon as it is kept by the HMT with at least one SE / configuration. The value assigned to it by the HMT is then computed as the highest one provided by the valuation step for all configurations that make the pixel fit. Valuation can be computed as the highest valuation among the configurations for which the pixel fits.

Unfortunately, ensuring invariance to scale and rotation through the HMT computing on a complete set of SE representing the various configurations is not efficient. Indeed, in the case of  $N$  possible configurations (or SE), HMT-based template matching will require  $N$  times the processing time required for a single SE. This is a strong bottleneck, which may be overcome by using several optimizations to be discussed later in this section. Moreover, in case of larger SE to deal with closer range images, the computation time will greatly increase. In this case, another solution consists in subsampling / interpolating the image instead of the template, before applying the HMT. Finally, particular attention should be given to the new templates generated from the input one, to avoid unexpected effects brought by discretization for instance.

### ***1.5.2 Dealing with Noise and Uncertainties***

Furthermore, as the HMT attempts to perform an exact match of the given pattern, it becomes sensitive to noise, occlusions, and even to the slightest variations of the template shape. Consequently a series of approaches have been imagined, with the purpose of countering this drawback and increasing its practical interest.

Bloomberg and Maragos [9] proposed several solutions to improve robustness to noise and shape uncertainties. The first idea is to perform a subsampling of both image and SEs. This solution is attractive as it reduces small shape variations and saves computation time. Nevertheless it requires the resolution to be good enough so the subsampling will preserve major features of the shape. Another possibility is to perform a spatial decimation of the support of structural functions following a regular grid. The advantages of this method are the same as subsampling's ones, but it can be applied even at low resolution.

It is also possible to improve noise resistance of the HMT by first dilating both foreground and background before performing erosions, as proposed in the binary case by Bloomberg [9]. In this case the foreground and the background overlap, thus it becomes easier to fit the SEs. However the extension to the greyscale and color cases is not trivial since we have to define the structuring functions to be used.

Another way to improve robustness against noise and shape uncertainties is to provide less informative SEs (*i.e.* increase the distance between the foreground and the background). This is nearly equivalent to previous Bloomberg's method and can be the easiest way to work with low level signal-to-noise ratio. Nevertheless this method fails at very low SNR as the SEs become so blurred that almost every configurations can provide a good match.

A simple solution to improve the tolerance to impulsive noise of all methods is to use rank operators [31, 35] instead of traditional erosion and dilation [18, 9] (*i.e.* replace min and max by quantiles). This solution is described in detailed in section 1.5.2.1 in the case of VHMT. However this solution implies to determine an appropriate rank for both dilation and erosion operations. Khosravi and Schafer [18] have shown that a lower and upper bounds for the rank are given respectively by

impulsive and Gaussian noise, but they did not provide a general formula to obtain these bounds. They also concluded that the effect of rank operator on Gaussian or Poisson noise is limited. Later, Murray *et al.* [21] have proposed a general approach to automatically determine an optimal rank in the context of the HMT without any assumption on the noise distribution. In case of very noisy image, the Perret *et al.* fuzzy HMT [27] allows to recover good detection result.

Finally, some authors [7, 13] proposed to *learn* the foreground and background structuring elements from examples. This will be addressed in Sec. 1.5.4 but is also a way to incorporate the observed uncertainties in the definition of the templates. This latter approach called *synthetic* SE is described in section 1.5.2.1.

### 1.5.2.1 Practical Solutions in Color Images

While the methods proposed so far to deal with noise and uncertainties are mainly related to the general case of binary or greyscale images, we recall here the results from [6], namely rank order based VHMT and synthetic multivariate structuring functions.

#### Rank order based VHMT

A rank order filter of  $k^{\text{th}}$  rank is a transformation, where given a gray-level image  $F$  and a SE  $B$ , the result becomes:

$$(F \square_k B)(p) = k^{\text{th}} \text{ largest of } F(p+x), x \in B \quad (1.35)$$

with  $k \in \{1, \dots, |B|\}$ . Obviously,  $F \square_1 B = \delta_B(F)$  and  $F \square_{|B|} B = \varepsilon_B(F)$ . Moreover, always in the context of gray-level data, a rank order filter of  $k^{\text{th}}$  rank, is equivalent to the supremum of erosions using all possible SE with  $k$  points, and respectively to the infimum of dilations using all possible SE with  $|B| - k + 1$  points [36]. Due to this property, the binary HMT of Eq. (1.3) has been reformulated in the literature, by replacing the erosion in its expression with a rank order filter of rank  $k < |B|$ , hence making it possible to detect binary templates even in conditions of partial occlusion.

In order to achieve the same additional robustness in the case of a multivariate image  $\mathbf{F}$  along with a multivariate SF  $\mathbf{B}$  and a vector ordering  $\leq_v$ , one can redefine the rank order filter of  $k^{\text{th}}$  rank as follows:

$$\zeta_{\mathbf{B}}^k(\mathbf{F})(p) = k^{\text{th}} \text{ largest of } \mathbf{F}(p+x) - \mathbf{B}(x), x \in \text{supp}(\mathbf{B}) \quad (1.36)$$

$$\theta_{\mathbf{B}}^k(\mathbf{F})(p) = k^{\text{th}} \text{ largest of } \mathbf{F}(p-x) + \mathbf{B}(x), x \in \text{supp}(\mathbf{B}) \quad (1.37)$$

where  $k \in \{1, \dots, |\text{supp}(\mathbf{B})|\}$ . Naturally, the vectors are sorted using  $\leq_v$ . Thus,  $\varepsilon_{\mathbf{B}} = \zeta_{\mathbf{B}}^{|\text{supp}(\mathbf{B})|}$  and  $\delta_{\mathbf{B}} = \theta_{\mathbf{B}}^1$ . Consequently, one can now formulate an approximative VHMT, capable of detecting the sought template  $(\mathbf{V}, \mathbf{W})$  even if  $m$  and  $n$  pixels do not match respectively the foreground and the background:

$$\eta_{[V,W],m,n}^I(\mathbf{F})(p) = \begin{cases} \|\zeta_V^m(\mathbf{F})(p) - \theta_{W^*}^n(\mathbf{F})(p)\| & \text{if } \zeta_V^m(\mathbf{F})(p) >_v \theta_{W^*}^n(\mathbf{F})(p) \\ 0 & \text{otherwise.} \end{cases} \quad (1.38)$$

where  $m \in \{1, \dots, |\text{supp}(V)|\}$  and  $n \in \{1, \dots, |\text{supp}(W)|\}$ . It should also be noted that  $\eta_{[V,W],|\text{supp}(W)|,1}^I = \eta_{[V,W]}^I$ . Fig. 1.10 contains an example of the result given by this operator, where the leftmost image is sought under the same conditions as in Fig. 1.8. However, this time even though the right example has a red/brown stripe, it is still successfully detected. This is due to the use of the 750<sup>th</sup> rank, a number equal to the amount of different pixels between the two images. Thus the rank based operator can allow a flexibility margin large enough to realise the detection in case of pixel value variations, due to reasons such as noise.

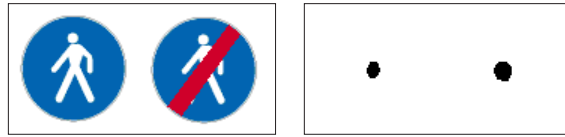


Fig. 1.10: On the left is a couple of images, of which the leftmost is the sought pattern, and on the right is the output of  $\eta_{[V,W],750,750}^I$ , Eq. (1.38) [6].

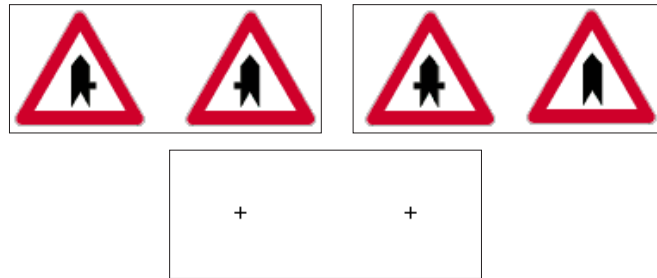


Fig. 1.11: In the first row, from left to right the two images to detect, and the corresponding lower and upper synthetic SF computed through Eqs. (1.39) and (1.40); the second row contains the result of VHMT, Eq. (1.21) [6].

### Synthetic Multivariate Structuring Functions

Although multivariate rank order filters make it possible to detect partial matches, Eq. (1.38) still hardly satisfies practical needs, since the objects corresponding to the sought template may vary considerably. Consider for instance the case illustrated in Fig. 1.11 (top-left). This situation is of course present in the context of detection from gray-level images as well. One way of countering it, as explained in [7, 13], is to employ a set of example images, from which a common template is formed, or as defined in Ref. [13], “synthetic”.

More precisely, the foreground is represented by the minimum and the background by the maximum of the given set of examples ( $\{\mathbf{V}_i\}, \{\mathbf{W}_j\}$ ). Thus, in the multivariate case the same technique may be employed merely by using the chosen vector ordering  $\leq_v$ :

$$\mathbf{V}(x) = \inf_i \{\mathbf{V}_i(x)\} \quad (1.39)$$

$$\mathbf{W}(x) = \sup_j \{\mathbf{W}_j(x)\} \quad (1.40)$$

Returning to Fig. 1.11, it suffices to compute the templates corresponding to the images at the top-left by means of this operation, and the VHMT of Eq. (1.21) detects both successfully.

### 1.5.3 Performance

Relying on a naive implementation of the previous HMT definitions will lead to a template matching process of poor performance (*i.e.* very long processing time). We describe here various methods which are available to reduce the computation time of the HMT when used in template matching.

#### SE/SF decimation

One simple way to speed-up the HMT is to use decimated structuring elements or functions [10]. The idea here is to subsample in a regular manner the structuring elements/functions. Indeed, the HMT precision is robust to such subsampling while this greatly reduces the computation cost as the computation cost is directly linked to the number of SE/SF pixels.

#### Hard fitting

Binary HMT but also grayscale/color HMTs that rely on a hard fitting step can easily be speeded-up by taking advantage of this strong constraint. Such HMTs lead to

an efficient implementation of the fitting step (which is in fact the most important part of HMT based template matching). In the case the fitting process requires a pixel to fit all the structuring elements/functions to be kept, it is relevant to stop the process as soon as one of the SE/SF pixel is not matched by the HMT. Only an incomplete processing of the set of SEs/SFs is then performed, thus greatly reducing the computing time.

### 1.5.4 Parameters Settings

The settings of the SE parameters may sometimes be tricky. In a given domain, it is expected to be made by an expert based on his domain knowledge. We consider here the context of remote sensing, for which several template matching attempts have been made with the HMT operator. In this context, and more precisely for coastline extraction, the expert knows (at least partially) the spectral signature of the desired object and how it can be distinguished from its environment. This spectral information depends on the type of sensor and eventually external factors (e.g., season for remote sensing imagery). To avoid computational inefficiency, it is better not to use all possible constraints, but to rather consider only the most discriminant spectral information of the object under study when compared to its environment. For instance, if we consider spectral knowledge given in Table 1.1, we can observe an important overlap of spectral signatures of sea and land in bands *Green* and *Red*. Thus, the expert will most probably not use these spectral bands as discriminative information in the template matching process. Setting parameters w.r.t. bands *Blue* and *Near-Infrared* looks much more relevant since the related information is more reliable to distinguish between sea and land.

Band	Sea	Land
<i>Blue</i>	173 – 193	134 – 165
<i>Green</i>	215 – 269	147 – 241
<i>Red</i>	119 – 167	66 – 177
<i>Near Infrared</i>	55 – 84	126 – 575

Table 1.1: Spectral ranges from sea and land obtained from a QuickBird image [38].

To ease the SE parameter setting step, intuitive and interactive approaches may be considered, *e.g.*, drawing scribbles on objects of interest [12, 39]. It then allows to learn the spectral range of the desired features and to automatically set the SE parameters in order to achieve the highest discriminative power of the template matching method. This principle is illustrated in Fig. 1.12 where the user has drawn markers on two warehouses and on the background: from this user input, the system is able to obtain the spectral range of the templates defined from the scribbles (Tab. 1.2). This can then help to feed a subsequent HMT template matching solution,

such as the knowledge-based multivariate HMT [38]. In this case, either the user analyzes the provided spectral ranges to select appropriate bands and thresholds, or a machine learning algorithm is involved to identify the best decision functions.

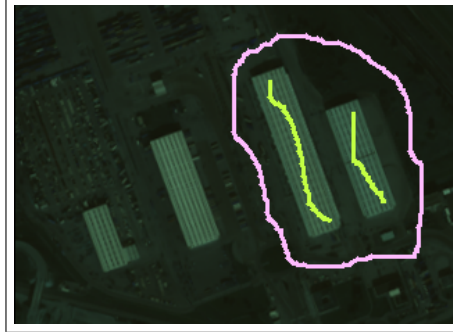


Fig. 1.12: Scribbles drawn on some warehouses and background to learn SE parameters from a QuickBird Image (©Digitalglobe) [38].

Besides the learning or definition of the spectral information of a multivariate/color template, the shape has also to be set and once again, interactive methods may be useful to get some rough ideas about the template sought by the user.

Band	Warehouses	Background
<i>Blue</i>	336 – 556	142 – 323
<i>Green</i>	511 – 857	161 – 476
<i>Red</i>	381 – 635	82 – 344
<i>Near Infrared</i>	362 – 612	93 – 431

Table 1.2: Spectral range of the scribbles drawn by the user on figure 1.12 [38].

### 1.5.5 From HMT to Template Matching

We have already addressed a set of issues raised when considering HMT on real images for template matching. To be successfully applied, morphological template matching also requires to be adapted to the specificities of the desired pattern. We can distinguish between two types of patterns which will now be discussed.

### 1.5.5.1 Discontinuity

Discontinuity is somehow an abstract feature: indeed, it is not considered as a straight visual feature but rather denotes the limit between two specific areas. Discontinuity extraction may be observed in general cases (*e.g.*, edge detection) but also in very specific ones (*e.g.*, coastline delineation). Here a strong assumption is made about the existence of two opposite SEs, each of them defining one given area. HMT based template matching dedicated to particular discontinuity extraction is usually built in two steps:

- The two areas have to be defined fully defined (with spatial and color/spectral information), but the spatial definition may be limited to the depth or width of the feature only.
- Apart for the detection of a specific directional discontinuity (*e.g.*, only vertical discontinuity), it is necessary to apply the HMT with different SE orientations.

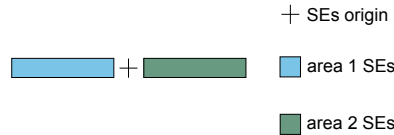


Fig. 1.13: Example of SEs for an oriented discontinuity extraction [38].

We notice that nothing prevents the two SEs to be unconnected. In this favorable case, the HMT operator is able to handle an uncertainty area.

### 1.5.5.2 Object

Object may be seen as the classical feature of template matching. Relying on any HMT operator, specific object extraction is achieved using two SEs: one is defining the object (being possibly as small as a single point) while the other is defining what is not the object (*e.g.*, the background, the object surrounding, etc.). The following steps are here necessary:

- The SE representing the object is fully defined, as well as the SE dedicated to background
- Depending of the object and its properties (fixed size or not, fixed orientation or not, etc.), the HMT has to be applied with SEs at various orientations and/or scales.

In order to be able to match the object even with discretization artefacts (*e.g.*, stairing effect), an uncertainty area located between the two SEs might be necessary.

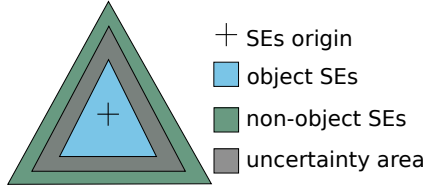


Fig. 1.14: Example of SEs for object extraction [38].

## 1.6 Applications

The relevance of the HMT as a solution for template matching is illustrated by several practical applications to help the reader understand the benefit of this operator when dealing with real-life problems. In this section, we present in particular some examples related to the fields of astronomical imaging [27], earth observation [20, 38, 37], document processing [40] and medical imagery [24]. Only a part of these examples are related to color images, since color HMT has been addressed only very recently. Nevertheless, nothing prevents the extension of the presented use cases to color data.

### 1.6.1 Astronomy: Low Surface Brightness Galaxy Detection

Galaxies come in various shapes but have long been expected to all have the same surface brightness. It's only recently that low surface brightness (LSB) galaxies (Fig. 1.15) have been discovered which leads to the problem of the automatic detection of these objects among the huge astronomical image datasets. In this subsection

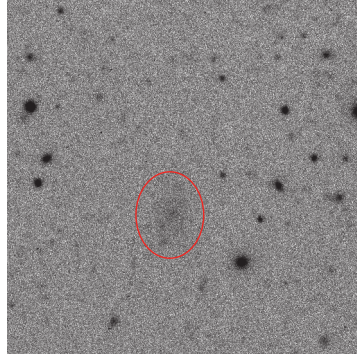


Fig. 1.15: Example of low surface brightness galaxy (inside the red ellipse) [27].

we describe a method based on PHMT (Eq. 1.16 page 8) to automatically build a segmentation map of potential LSB galaxies. This method has been presented in more details in [27]. The algorithm is decomposed into several steps. First it is necessary to build several patterns corresponding to LSB galaxies of various shapes and orientations. Because the sought objects are very close to the background in terms of photometry, a precise map of the background has also to be computed (*i.e.* evaluate the intrinsic luminosity of the sky at all points.) Next the original image is preprocessed with a median filter to reduce noise. Filtered image, background map, and pattern set are then used to calculate PHMT. The result is thresholded and the original shape of LSB galaxies is reconstructed.

### Description of Patterns

LSB galaxies can be modeled by a quite simple function that can be used to generate patterns of LSB galaxies. This model involves four parameters: the central brightness, the elongation, the orientation and the scale length. 10 possible scale-lengths and 14 orientations between 0 and  $\pi$  are considered. The final set of SEs obtained by combining all possible scale lengths, elongations and orientations while avoiding identical cases induced by symmetries, is composed of 640 templates (Fig. 1.16). Finally each pattern is composed of two SEs of same orientation and elongation.

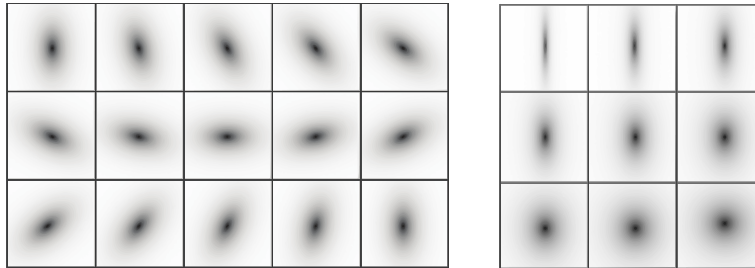


Fig. 1.16: Example of SEs obtained with a variation of orientations (left) and elongation (right) [27].

### Computation of PHMT

The PHMT of each pair of structuring elements is computed for each pixel and the best matching score is stored in a so called *score map* (Fig. 1.17). In the next step, the score map is thresholded. As all parameters of the algorithm are set automatically according to observation parameters and statistics, the score gives an absolute measure which is independent of the observation and the use of the same threshold for every observation is not a problem. Finally, each pixel of the binary map is

dilated by the support of the pattern that gives the maximum score in this position (Fig. 1.17).

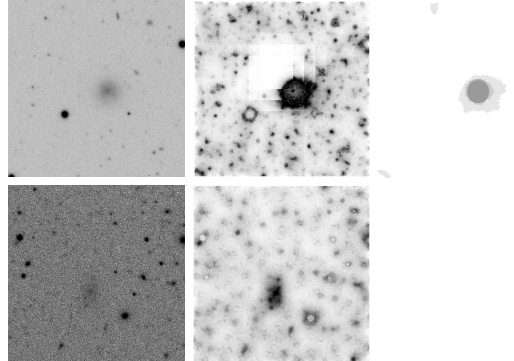


Fig. 1.17: Application of the PHMT to LSB galaxy detection [27]. First column: original image. Second column: score map obtained after application of the PHMT (the blocky aspect comes from the background and noise estimation procedure that is done on a subgrid of the original image). Third column: thresholded and reconstructed map. The final map contains different classes proportional to the object brightness. This allows deblending capabilities for overlapping objects having different brightnesses.

## Experiments

The robustness of the method has been assessed by extensive testing on simulated and real datasets. The evaluation obtained on more than a thousand simulated images have shown that the method is able to detect LSB galaxies down to a peak signal-to-noise ratio of 0 dB even in relatively crowded environment (inducing overlapping). These good results have been reproduced on two real images ( $2048 \times 4096$  pixels) where the algorithm proposed 23 candidates, among which 6 were already known LSB galaxies, 8 were new LSB galaxies and the others were false positives.

### **1.6.2 Earth Observation: Natural and Human-made Objects Extraction**

#### **1.6.2.1 Coastline extraction**

As a first application example in earth observation through remote sensing, we consider the case of satellite images with a very high spatial resolution (VHR). Template

matching on such images can focus on some predefined borders, coastline being one of the most representative examples when dealing with coastal remote sensing.

The sought template considered here is rather particular since it is indeed a discontinuity, as coastline is typically defined as the border between sea and land. Its automatic extraction from digital image processing is a very topical issue in remote sensing imagery [11]. Even if some methods have been proposed for low or medium spatial resolution, none are relevant on very high spatial resolution (VHR) satellite imagery where a pixel represents an area lower than  $5 \times 5 m^2$ .

Since a coastline is well defined both with spatial and spectral information, the KHMT can be seen as a relevant tool to perform its extraction. A basic assumption would be that only two SEs are necessary to identify the two parts around the border (*i.e.* sea and land) as shown by  $S^1$  and  $S^2$  in Figure 1.18. However, to be able to distinguish between coastlines and other water-land borders (*e.g.*, lake border, river bank, etc), an additional SE is involved to represent deep sea (or at least water further from the coastline) as illustrated by  $S^3$  in Figure 1.18.

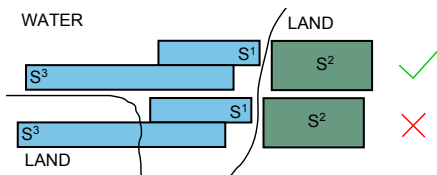


Fig. 1.18: Spatial definition of SEs used for coastline extraction with matching and unmatching conditions [38]

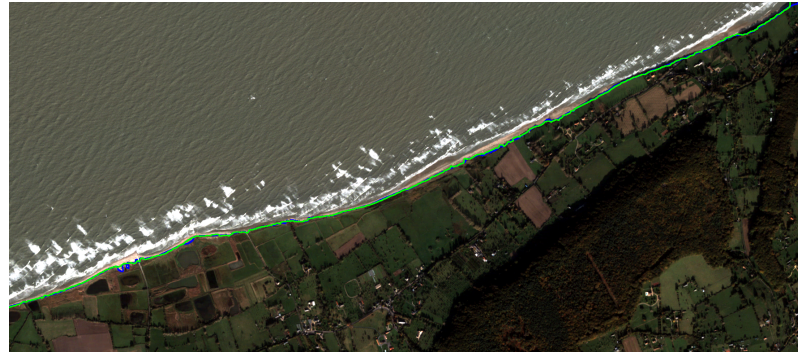


Fig. 1.19: Coastline extraction on Normandy coast from a QuickBird image (©Digitalglobe), extracted coastline in green and reference coastline in blue (results are dilated for better visualization) [38].

The relevance of KHMT for the extraction of coastline in VHR imagery can be observed in Fig. 1.19. The interested reader will find more details in [28, 38].

### 1.6.2.2 Tank extraction

In [38], another application in earth observation is presented to deal with petroleum tank extraction. On a study site located in the harbor of Le Havre in France, such petroleum tanks are cylindric (like other tanks) but are also white (which make them distinguishable from other tanks). In this context, spatial information needs to be combined with spectral information to ensure an accurate detection of these objects. KHMT then appears as a relevant solution, using two sets of SEs: one defining the petroleum tanks, and the other defining their neighbourhood. Their shapes are shown in figure 1.20.

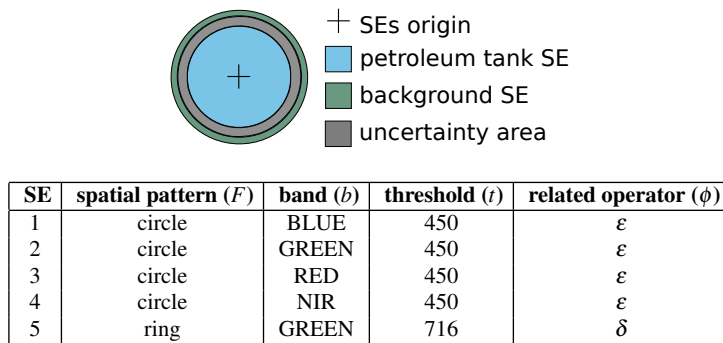


Fig. 1.20: Spatial definition of SEs used for petroleum tank extraction and corresponding SEs definition [38]. Pixel values are encoded with 11 bits per band (range is [0;2047]) and extracted from Quickbird sensor.

Since there is not a unique size for petroleum tanks, KHMT has to be applied with various SE sizes. The spectral parameters are defined by an expert and given in Fig. 1.20. The spatial parameters are the following: the circular SE is of radius  $r$  varying from 5 to 20 pixels, while the surrounding ring SE radius is a little bit larger (*i.e.* equal to  $r + 2$ ) and ring width is 1 pixel.

Shape *circle* represents object set of SEs while *ring* represents non-object set of SEs. NIR means Near Infra-Red band. In this example, thresholds have been easily set by the expert from a manual study of the multispectral image histogram. Indeed, tanks might be distinguished from the other objects and the image background based on their spectral signature. Peak values in the histogram are used to set adequate threshold values.

Applying KHMT with these parameters gives promising results as shown in Fig. 1.21. This satellite image contains 33 petroleum tanks, 32 were extracted, one was missed due to the presence of dark colors on its roof and there is no false positive. KHMT appears here as an efficient solution to deal with the problem of specific tank extraction. Let us note that the problem of the missed tank can be further solved by introducing some robustness in the KHMT operator, as it has been discussed previously with some other HMT definitions.



Fig. 1.21: Petroleum tank extraction on Le Havre harbor QuickBird image(©Digitalglobe) [38]. Correct detections are surrounded by white boundary, false negative are given in cyan (there is no false positive).

### 1.6.2.3 Building extraction

The last example in the field of earth observation focuses on automatic building extraction, which is helpful to optimize the management of urban space by local politics. The overall approach presented here [20] is composed of three main steps: (1) binarization/clustering of the input grayscale image (here a panchromatic Quickbird image) to obtain a map of relevant features and make the data compatible with a binary HMT operator; (2) prefilter the binary images using morphological filters for which parameters (SE properties) are obtained automatically from morphological image analysis step; (3) proceed to building extraction using an adaptive HMT.

This approach assumes that building roofs are of rectangular shape, and made of homogeneous content (or at least of several homogeneous parts). In this context, it is expected that binary images produced from the two first steps either contain entire building roofs, or significant parts of them, which are further recombined with a “combination and fusion of clusters” step. This last case can be explained by the variations brought by different roof materials and sunlight illuminations, as illustrated by Fig. 1.22 where we can observe the relevance of combining various clusters to build meaningful binary images to be processed by the HMT. The HMT is then adapted to various sizes (width and length of the rectangular SE, see previous section) to deal with the different configurations of rectangular-shaped buildings observed from remote sensing imagery. Similarly to previous approach, the last step consists of a (geodesic) reconstruction to obtain the identified buildings from the fitted pixels.

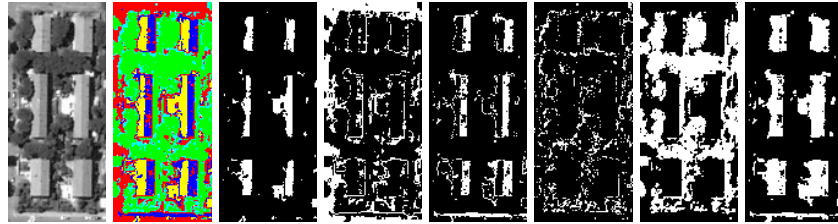


Fig. 1.22: Processing with the HMT a clustering result as a set of binary images [20]: (from left to right) input image, clustering, binary images corresponding to the 5 clusters, and the binary image obtained by merging clusters 1 and 3.

An illustration of this building extraction scheme is given in Fig. 1.23. We can observe the relevance of the HMT operator w.r.t assumptions made (building roof is made of a single homogeneous part or of an heterogeneous set of different homogeneous roof parts), as well as the limits of such assumptions (in case of highly heterogeneous roofs).

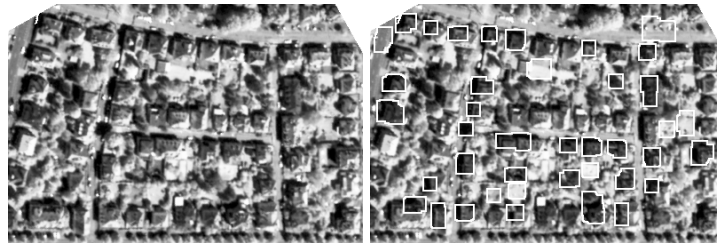


Fig. 1.23: Illustration of building extraction [20]: input image (left), and final result (bottom right).

#### 1.6.2.4 Ship detection

Velasco-Forero and Angulo use their color HMT based on supervised ordering to detect ships in color satellite image [37]. The input RGB image is taken from the WorldView-2 satellite, with a spatial resolution of 50cm per pixel. Ships are made of grayish pixels on a blue background representing the sea. In this context, learning an ordering to distinguish between blue and grey pixels is relevant, and help the method to reach high detection rates.

### ***1.6.3 Document : Symbol spotting in architectural plan***

Symbol spotting is an emerging topic and few works haven been proposed so far. Although well-known symbol descriptors work well to describe isolated symbols, their performance in real applications drop away when symbols are embedded in documents. In the context of monosize symbol (*e.g.*, architectural plan), HMT-based methods are particularly adapted to symbol spotting and we recall here results presented in [40].

The major symbol spotting difficulty when dealing with plan images is the overlapping/occlusion of symbols which are embedded into the document and make harder their spotting. To achieve the robustness to information overlapping, Weber and Tabbone do not rely on a fitting step but rather provide for every pixel two different matching scores. These scores are respectively dedicated to the foreground and the background, assuming a perfect match with the foreground while being less strict with the background due to information overlap. More precisely, the foreground (resp. background) matching score is defined as the mean of foreground (resp. background) pixel matching scores. This foreground (resp. background) pixel matching score is set to 1 if the pixel value is greater or equal (resp. lower or equal) to the corresponding foreground (resp. background) pixel, and to a value in  $[0; 1[$  otherwise (to ensure robustness to small value differences). As with other applications, geometric robustness (*w.r.t* orientation, symmetry) is achieved through the application of the HMT in various configurations.

Figure 1.24 illustrates the spotting efficiency of this approach in complex overlapping situations. We can observe that: (1) HMT is able to spot a symbol even if it is connected to another symbol; (2) HMT is able to extract a symbol even if it is highly overlapped by other information; and (3) HMT comes with a high discrimination power since it can spot the queried symbol and not the other but very similar symbols.

### ***1.6.4 Medical: Feature Extraction for Pathology Detection***

#### **1.6.4.1 Vessel segmentation**

The spread of medical images from different types (MRI, CT, ...) had led to the need of segmentation techniques adapted to the particular content of these data. In this context, vessels have been a successful target of HMT-based template matching. Indeed, using foreground and background structuring functions is particularly adapted to the invariant vessel properties in terms of shape and intensity. HMT can then be used directly as a vessel extractor or as voxel “vesselness” indicator [24].

The structuring functions to be used aim to match the “cylindrical” shape of vessels (both the vessel itself and its close neighborhood). In order to deal with vessels with different sizes and orientations, a whole set of SFs should be used. Moreover, computation time is reduced by using decimated SF (cf. section 1.5).

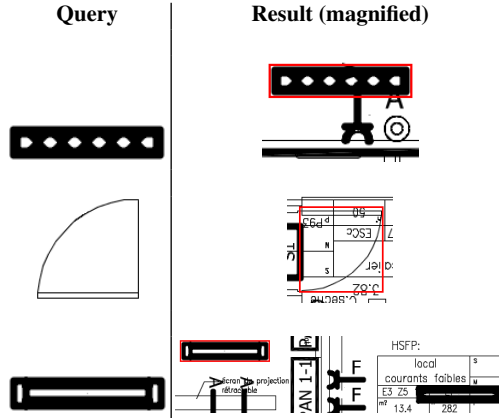


Fig. 1.24: Difficult spotting cases, from top to bottom: connected symbols, overlapped symbols, similar symbols [40]. The sought template is given on the left, the magnified result provided by the HMT on the right.

This approach gives excellent results. It obtains a detection rate of 100% for the entrance of the liver portal vein [25] and better results than other methods on brain vessels extraction [26].

#### 1.6.4.2 Rosacea detection

The color HMT elaborated by Ledoux *et al.* [19] has been applied to skin image analysis. The goal is to detect specific lesions (rosacea). To do so, the reference colors have been set statistically and the sought template's bounds have been set manually. The preliminary results obtained by the authors call for further exploration of the HMT to extract complex color shapes in dermatology.

## 1.7 Conclusion

Template matching is a fundamental problem in image analysis and computer vision. It has been addressed very early by Mathematical Morphology, through the well-known Hit-or-Miss Transform. In this chapter, we review most of the existing works on this morphological template matching operator, from the standard case of binary image to the (not so standard) case of grayscale images and the very recent extensions to color and multivariate data. We also discuss the issues raised by the application of the HMT operator in the context of template matching and provide guidelines to the interested reader. Various use cases in different application domains have been provided to illustrate the potential impact of this operator.

While having successfully addressed various real template matching problems, HMT still suffers from some drawbacks which are calling for future work in the field. Among the main issues, we would like to underline the computational complexity of the HMT operator, especially when dealing with multiple templates (SE) to ensure orientation and scale invariance. Besides, adequately defining templates as structuring elements is often tricky and not enough intuitive. We believe that machine learning can be of great help to determine the template or set of templates to be used in the matching process. Finally, while having already benefited from several attempts to increase robustness to uncertainties, too many HMT based template matching methods are limited by the strong constraints brought by the underlying HMT definition. This has prevented the wide dissemination of the HMT as a powerful, reliable and theoretically sound template matching operator.

## References

1. Angulo, J., Lefèvre, S., Lézoray, O.: Color representation and processing in polar color spaces. In: C. Fernandez-Maloigne, F. Robert-Inacio, L. Macaire (eds.) Numerical Color Imaging, pp. 1–40. ISTE – Wiley (2012)
2. Aptoula, E., Lefèvre, S.: A comparative study on multivariate mathematical morphology. *Pattern Recognition* **40**(11), 2914–2929 (2007)
3. Aptoula, E., Lefèvre, S.: On lexicographical ordering in multivariate mathematical morphology. *Pattern Recognition Letters* **29**(2), 109–118 (2008)
4. Aptoula, E., Lefèvre, S.: Multivariate mathematical morphology applied to colour image analysis. In: C. Collet, J. Chanussot, K. Chehdi (eds.) Multivariate image processing: methods and applications, pp. 303–337. ISTE – John Wiley (2009)
5. Aptoula, E., Lefèvre, S.: Morphological texture description of grayscale and color images. In: P. Hawkes (ed.) Advances in Imaging and Electron Physics, vol. 169, pp. 1–74. Elsevier (2011)
6. Aptoula, E., Lefèvre, S., Ronse, C.: A hit-or-miss transform for multivariate images. *Pattern Recognition Letters* **30**(8), 760–764 (2009)
7. Barat, C., Ducottet, C., Jourlin, M.: Pattern matching using morphological probing. In: Proceedings of the 10th International Conference on Image Processing, vol. 1, pp. 369–372. Barcelona, Spain (2003)
8. Barat, C., Ducottet, C., Jourlin, M.: Virtual double-sided image probing: a unifying framework for non-linear grayscale pattern matching. *Pattern Recognition* **43**, 3433–3447 (2010)
9. Bloomberg, D.S., Maragos, P.: Generalized hit-miss operations. In: SPIE Conference 1350, Image Algebra and Morphological Image Processing, pp. 116–128. San Diego, CA (1990)
10. Bloomberg, D.S., Vincent, L.: Pattern matching using the blur hit-miss transform. *Journal of Electronic Imaging* **9**, 140–150 (2000)
11. Boak, E., Turner, I.: Shoreline definition and detection: a review. *Journal of Coastal Research* **21**(4), 688–703 (2005)
12. Boykov, Y.Y., Jolly, M.P.: Interactive graph cuts for optimal boundary & region segmentation of objects in n-d images. In: IEEE International Conference on Computer Vision, vol. 1, pp. 105–112 (2001)
13. Doh, Y., Kim, J., Kim, J., Kim, S., Alam, M.: New morphological detection algorithm based on the hit-miss transform. *Optical Engineering* **41**(1), 26–31 (2002)
14. Goutsias, J., Heijmans, H.J.A.M., Sivakumar, K.: Morphological operators for image sequences. *Computer Vision and Image Understanding* **62**(3), 326–346 (1995)
15. Heijmans, H., Serra, J.: Convergence, continuity and iteration in mathematical morphology. *Journal of Visual Communication and Image Representation* **3**(1), 84–102 (1992)

16. Heijmans, H.J.A.M.: Morphological Image Operators. Advances in Electronics and Electron Physics Series. Academic Press, Boston (1994)
17. Heijmans, H.J.A.M., Ronse, C.: The algebraic basis of mathematical morphology, part I: dilations and erosions. Computer Vision, Graphics and Image Processing **50**(3), 245–295 (1990)
18. Khosravi, M., Schafer, R.: Template matching based on a grayscale hit-or-miss transform. IEEE Transactions on Image Processing **5**(5), 1060–1066 (1996)
19. Ledoux, A., Richard, N., Capelle-Laizé, A.: Color hit-or-miss transform (cmomp). In: EURASIP European Conference on Signal Processing (EUSIPCO), pp. 2248–2252. Bucharest, Romania (2012)
20. Lefèvre, S., Weber, J., Sheeren, D.: Automatic building extraction in VHR images using advanced morphological operators. In: IEEE/ISPRS Joint Workshop on Remote Sensing and Data Fusion over Urban Areas. Paris, France (2007)
21. Murray, P., Marshall, S.: A new design tool for feature extraction in noisy images based on grayscale hit-or-miss transforms. IEEE Transactions on Image Processing **20**(7), 1938–1948 (2011)
22. Murray, P., Marshall, S.: A review of recent advances in the hit-or-miss transform. In: P.W. Hawkes (ed.) Advances in Imaging and Electron Physics, vol. 175, pp. 221–282. Elsevier (2013)
23. Naegel, B., Passat, N., Ronse, C.: Grey-level hit-or-miss transforms – part I: Unified theory. Pattern Recognition **40**(2), 635–647 (2007)
24. Naegel, B., Passat, N., Ronse, C.: Grey-level hit-or-miss transforms – part II: Application to angiographic image processing. Pattern Recognition **40**(2), 648–658 (2007)
25. Naegel, B., Ronse, C., Soler, L.: Using grey-scale hit-or-miss transform for segmenting the portal network of the liver. In: ISMM 2005 - 7th International Symposium on Mathematical Morphology, Proc., *Computational Imaging and Vision*, vol. 30, pp. 429–440. Springer SBM (2005)
26. Passat, N., Ronse, C., Baruthio, J., Armspach, J.P., Maillot, C.: Magnetic resonance angiography: From anatomical knowledge modeling to vessel segmentation. Medical Image Analysis **10**(2), 259 – 274 (2006)
27. Perret, B., Lefèvre, S., Collet, C.: A robust hit-or-miss transform for template matching in very noisy astronomical images. Pattern Recognition **42**(11), 2470–2480 (2009)
28. Puissant, A., Lefèvre, S., Weber, J.: Coastline extraction in vhr imagery using mathematical morphology with spatial and spectral knowledge. In: XXIth ISPRS Congress - Beijing (2008)
29. Raducanu, B., Grana, M.: A grayscale hit-or-miss transform based on level sets. In: Proceedings of the 7th International Conference on Image Processing, vol. 2, pp. 931–933. Vancouver, Canada (2000)
30. Ronse, C.: Why mathematical morphology needs complete lattices. Signal Processing **21**(2), 129–154 (1990)
31. Ronse, C.: A lattice-theoretical morphological view on template extraction in images. Journal of Visual Communication and Image Representation **7**(3), 273–295 (1996)
32. Schaefer, R., Casasent, D.: Nonlinear optical hit-miss transform for detection. Applied Optics **34**(20), 3869–3882 (1995)
33. Serra, J.: Anamorphoses and function lattices. In: E.R. Dougherty (ed.) Mathematical Morphology in Image Processing”, chap. 13, pp. 483–523. Marcel Dekker, New York (1993)
34. Soille, P.: Advances in the analysis of topographic features on discrete images. In: Proceedings of the 10th International Conference on Discrete Geometry for Computer Imagery DGCI'02, *Lecture Notes in Computer Sciences*, vol. 2301, pp. 175–186 (2002)
35. Soille, P.: On morphological operators based on rank filters. Pattern Recognition **35**(2), 527–535 (2002)
36. Soille, P.: Morphological Image Analysis: Principles and Applications. Springer, Berlin (2003)
37. Velasco-Forero, S., Angulo, J.: Hit-or-miss transform in multivariate images. In: Advanced Concepts for Intelligent Vision Systems, *Lecture Notes in Computer Sciences*, vol. 6474, pp. 452–463. Springer Verlag (2010)

38. Weber, J., Lefèvre, S.: Spatial & spectral morphological template matching. *Image and Vision Computing* **30**(12), 934–945 (2012)
39. Weber, J., Lefèvre, S., Gancarski, P.: Interactive Video Segmentation based on Quasi-Flat Zones. In: Proceedings of IEEE International Symposium on Image and Signal Processing and Analysis, pp. 265–270. IEEE, France (2011)
40. Weber, J., Tabbone, S.: Symbol spotting for technical documents: An efficient template-matching approach. In: International Conference on Pattern Recognition (ICPR). Tsukuba, Japan (2012)